ChemComm

COMMUNICATION

Check for updates

Integrating salen complexes into gas diffusion electrodes for CO_2 electroreduction: considerations for employing molecular precatalysts in heterogeneous electrolyzers
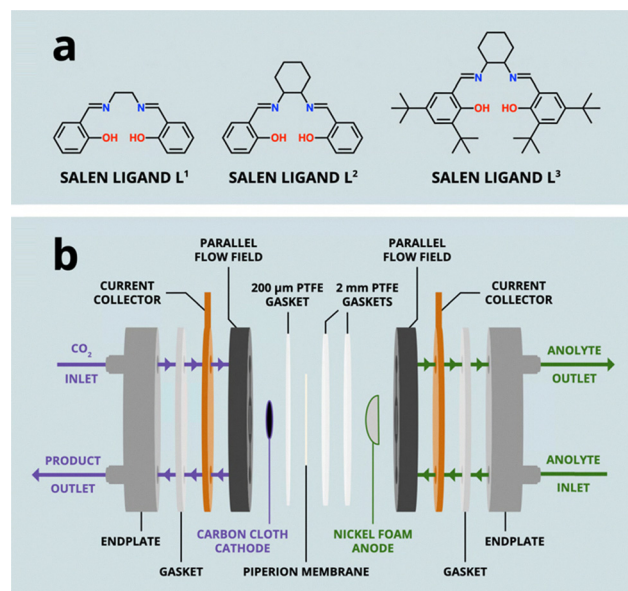
Dana M. Feldman, [ID] [ab] Kevinjeorjios Pellumbi, [ID] [c] Igor Zimmermann,[c] Wiebke Wiesner,[a] Sebastian A. Sanden,[a] Simon C. B. Suhr,[b] Patrick L. Holland [ID] [b] and Ulf-Peter Apfel [ID] ★[ac]

Transition metal salen complexes (Co, Ni, Cu) are studied as pre-catalysts for CO_2-to-CO electroreduction in zero-gap electrolyzers. Performance depends strongly on metal choice and electrode characteristics. XPS, UV-Vis, comparisons to simple metal salts, and a RHE-ZGE half-cell setup shed light on precatalyst decomposition and inform methodologies for molecular electrocatalyst heterogenization.

With the current shift towards more sustainable synthetic pathways, CO_2 electrolysis has gained attention as a promising technology. Beyond established Ag-, Au-, and Zn-based catalysts, numerous molecular systems have demonstrated high faradaic efficiencies for CO_2-to-CO conversion.[1,2] However, the majority of catalysts conceptualized in lab environments fail to make the transition into industrial reactors.[3] Bridging this "Valley of Death" for new electrolytic materials, as previously described by our group, requires an application-oriented strategy that couples catalyst development with process optimization in scalable devices, like zero-gap electrolyzers (ZGEs), that enable CO_2 electrolysis at elevated current densities.[4] For molecular electrocatalysts in particular, the tools available to achieve this transfer to industrially relevant ZGEs remain highly limited.[2,5] We thus set out to identify key experimental considerations for incorporating molecular electrocatalysts into gas diffusion electrodes (GDEs) for CO_2 reduction in ZGEs. We chose to focus our research on salen complexes, which are affordable, modular, compatible with a wide range of non-precious metals, and have shown good CO_2 electroreduction activity in both homogeneous and heterogeneous reaction environments.[5–10] Specifically, we aimed to: (1) study how ink

preparation and operating conditions affect CO_2R activity to find optimized process parameters, (2) determine the influence of different metal centers (Co, Ni, Cu) and salen ligands on CO_2R performance under those optimized process parameters, and (3) use pre- and post-electrolysis surface XPS to identify possible salen complex decomposition occurring after drop-casting or after electrolysis.

The three salen ligands used in this research are illustrated in Fig. 1a. All salen complexes of Co^{II}, Ni^{II}, and Cu^{II} used herein are described by the symbol of the metal and the name of the salen ligand used; for instance, the salen complex with a Co center using ligand L^2 is described as "CoL^2." All GDEs were prepared by directly adding solid catalyst, powdered carbon

[a] Fakultät für Chemie und Biochemie, Anorganische Chemie I, Ruhr-Universität Bochum, Universitätsstraße 150, 44801 Bochum, Germany. E-mail: ulf.apfel@rub.de

[b] Department of Chemistry, Yale University, 225 Prospect Street, New Haven, Connecticut 06511, USA

[c] Department for Electrosynthesis, Fraunhofer UMSICHT, Osterfelder Straße 3, 46047 Oberhausen, Germany

Fig. 1 (a) The salen ligands (L^1, L^2, and L^3) used in this work. (b) Diagram of the internal components of the zero-gap electrolyzer (ZGE) used in this research, including the gas diffusion electrode (carbon cloth cathode).

black, and PTFE nanoparticles (where noted) to a vial, sonicating in ethanol or THF, adding Sustainion® XA-9 alkaline ionomer, and then dropcasting the resulting ink onto a carbon cloth electrode at 70 °C until a catalyst loading of 0.45 mg cm^{-2} was achieved. These electrodes were then used as cathodes inside a ZGE (design shown in Fig. 1b). During operation, an aqueous 1 M KOH anolyte solution was circulated through the anode side of the ZGE, while CO_2 was passed through a 2 cm^2 parallel flow field on the cathode side employing a PiperION® anion-exchange membrane (AEM) at room temperature, as previously reported.[11–13] After an operating period of 30 minutes, any gaseous products (CO, CH_4, C_2H_4, and H_2) generated by the cell were analyzed by an in-line GC system. Further details regarding equipment and procedures can be found in the SI.

The commercially available cobalt salen complex CoL^2 was chosen for process parameter optimization experiments, as we expected that the hydrophobic and electronic properties of ligand L^2 would represent a reasonable medium of the hydrophobic and electronic properties of ligands L^1 and L^3. Preliminary experiments were conducted at a current density of 100 mA cm^{-2} with either humidified or non-humidified CO_2 feeding the cathode (Table 1a). Our experiments with non-humidified CO_2 showed a slightly higher average FE$_{CO}$ value

of 4% – with the remaining amount of charge being consumed in parasitic hydrogen evolution, as verified by GC analysis (Table S2) – while experiments with humidified CO_2 generated an FE$_{CO}$ of only 1%. This led us to suspect that moisture accumulation at the cathode might hinder CO_2R activity. Even when non-humidified CO_2 is used, the GDE is still wetted by water transport through the AEM, so we sought to directly control moisture content at the cathode through the incorporation of hydrophobic materials. To this end, varying amounts of hydrophobic PTFE nanoparticles (0.5, 1.0, 2.5, and 5.0 mg cm^{-2}) were added to the catalyst ink prior to dropcasting (Table 1b).[14] Electrolyses at a lower current density of 50 mA cm^{-2} showed that the amount of PTFE added does not affect FE$_{CO}$. Additionally, seeking to understand whether the carbon support added to the ink plays a role in CO_2R performance, we tested five different varieties of carbon supports (Ensaco® 250G, Super P® Li, C-Nergy® Super C65, Vulcan® XC-72R, and multi-walled carbon nanotubes) (Table 1c). Operating at 50 mA cm^{-2}, Ensaco® 250G gave the highest average FE$_{CO}$ values, followed by Super P® Li alongside C-Nergy® Super C65. This trend is in line with previous results from our group on molecular Ag catalysts in which the hydrophobic and graphitic character of Ensaco® 250G appears to promote CO_2R.[9,12] Variations in carbon porosity and particle size may influence the formation of distinct microenvironments with locally altered water activity, potentially facilitating decomposition and hydroxylation of the salen complexes to other active species, as evidenced by our pre- and post-electrolysis XPS analyses (to be discussed later).[15] The fact that CO_2 humidification and the type of carbon black added had a significant influence on observed CO_2R performance – while the addition of PTFE nanoparticles did not – suggests that local water content at the GDE is best controlled either at the carbon-catalyst interface or at the macroscopic interface through operational conditions, such as relative CO_2 humidification or temperature.

Further experiments were carried out with Ensaco® 250G in which the catalyst loading of CoL^2 was kept constant while the amount of carbon black was varied. 0.5, 1.0, and 2.0 equivalents of carbon black by weight relative to the catalyst were tested (Table 1d). While the obtained FE$_{CO}$ values showed no significant dependence on the carbon-to-catalyst weight ratio, chronopotentiometry data from these trials showed that carbon-to-catalyst weight ratios of 1.0 and 2.0 often led to non-stabilized, elevated cell voltages of up to 4 V (Fig. S13–S17). This can be attributed to the increased amount of non-catalytically active carbon support (inactive towards both CO_2 reduction and water reduction) present in the GDE matrix. Decreasing the current density from 50 to 10 mA cm^{-2} causes the FE$_{CO}$ value of GDEs dropcast with CoL^2 to increase from 10% at 50 mA cm^{-2} to 41% at 10 mA cm^{-2} (Table 1e), where the change in FE$_{CO}$ is again compensated for by a change in FE$_{H_2}$, as verified by GC analysis (Table S2). Despite the limited performance of CoL^2 for CO_2 reduction at current densities above 50 mA cm^{-2}, our results show how process parameters related to ink preparation and cell operation (CO_2 humidification, addition of PTFE nanoparticles, and the type and amount of carbonaceous support)

Table 1 Results from process parameter optimization experiments with CoL^2. Unless otherwise indicated, all experiments were run with dry CO_2 at a current density of 50 mA cm^{-2}. Each reported FE$_{CO}$ value is the average of two separate trials, and the 95% C.I. from the mean is provided. Values of FE$_{H_2}$ and total FE values for these experiments, as well as further experimental details, are available in the SI (Table S2). All CO_2 humidification experiments were run at 100 mA cm^{-2}

(a) CO_2 Humidification (% relative humidification)	FE$_{CO}$ (%)
Dry CO_2 (0%)	3.68 ± 0.57
Humidified CO_2 (100%)	1.339 ± 0.081

(b) Amount of PTFE nanoparticles added (mg cm^{-2})	FE$_{CO}$ (%)
0.0	10.4 ± 2.5
0.5	10.5 ± 1.2
1.0	8.0 ± 1.2
2.5	8.48 ± 0.85
5.0	10.7 ± 3.6

(c) Type of carbon black added	FE$_{CO}$ (%)
Ensaco® 250G	10.4 ± 2.5
Super P® Li	7.06 ± 0.40
C-Nergy® Super C65	6.8 ± 1.7
Vulcan® XC-72R	4.8 ± 1.6
Multi-walled CNTs (Fe-free)	4.128 ± 0.083

(d) Carbon-to-catalyst weight ratio	FE$_{CO}$ (%)
0.5	10.4 ± 2.5
1.0	9.0 ± 1.3
2.0	7.8 ± 4.0

(e) Current density (mA cm^{-2})	FE$_{CO}$ (%)
10	41 ± 10
50	10.4 ± 2.5
100	3.68 ± 0.57

can impact faradaic efficiencies for CO production. More specifically, when screening heterogenized molecular electrocatalysts for CO_2 reduction on GDEs, we suggest employing non-humidified CO_2 streams and paying close attention to the variety and amount of carbon support incorporated into the catalyst ink, with more hydrophobic materials appearing the most promising.

Based on these process parameter optimization experiments, we chose to run all subsequent trials with non-humidified CO_2 at successive current densities of 10 mA cm^{-2}, 25 mA cm^{-2}, and 50 mA cm^{-2} using a catalyst ink prepared with Ensaco® 250G in a carbon-to-catalyst weight ratio of 0.5 and without any PTFE nanoparticles added. Experiments were conducted with different salen ligands, providing varying hydrophobic and electronic effects, as well as different metal centers. The resulting FE$_{CO}$ values are presented in Fig. 2a (at 10 mA cm^{-2}) and Fig. S22–S28 (all current densities) for Co salen complexes CoL^1, CoL^2, and CoL^3, Ni salen complexes NiL^1 and NiL^3, and Cu salen complexes CuL^1 and CuL^3. Ni and Cu complexes were not prepared with L^2, as this ligand (representing an intermediate between L^1 and L^3 in terms of hydrophobic and electronic effects) was used only for process parameter optimization. CoL^1 displays a high faradaic efficiency for CO production (FE$_{CO}$: 91%) at a current density of 10 mA cm^{-2}, yet this FE$_{CO}$ value drops precipitously with

increasing current density to 2% at 50 mA cm^{-2}. As described in the prior paragraph, CoL^2 follows a similar trend, giving a FE$_{CO}$ value of 41% at 10 mA cm^{-2} that decreases with rising current density, while CoL^3 shows no specific activity for the CO_2R. Moreover, both Ni salen complexes are almost entirely inactive towards CO_2 electroreduction, with GDEs dropcast with NiL^1 only producing small amounts of CO, even at very low current densities (FE$_{CO}$: 2% at 10 mA cm^{-2}) and NiL^3 GDEs almost exclusively producing H$_2$. These findings are in line with the poor activity observed for a Ni porphyrin complex under nearly identical conditions.[13] Notably, although CuL^1 and CuL^3 show lower FE$_{CO}$ values than CoL^1 and CoL^2 at 10 mA cm^{-2}, both Cu salen complexes display much smaller drops in their FE$_{CO}$ values as current density increases compared to CoL^1 and CoL^2: FE$_{CO}$ values for CoL^1 drop by 97% when current density is increased from 10 to 50 mA cm^{-2}, whereas FE$_{CO}$ values for CuL^1 drop by only 5% over the same increase in current density. CuL^3 is the only complex that produces CH$_4$, with an FE$_{CH_4}$ of 2% at 50 mA cm^{-2} and 4% at 100 mA cm^{-2}; no hydrocarbon products are observed for any of the other tested complexes.

Compared to reported systems involving molecular CO_2R electrocatalysts in heterogeneous electrolyzers (see Table S3), the salen complexes tested herein show limited activity for CO_2R on GDEs, despite promising CO_2R performance in homogeneous systems. As we have highlighted in a recent review,[16] the incorporation of molecular electrocatalysts into ZGEs requires *in situ* spectroscopic studies to best identify the catalytically active species (if any) that are formed on the electrode before and after electrolysis.[2] To assess possible salen complex decomposition, XPS surface scans were collected of pre- and post-electrolysis GDEs dropcast with CoL^2, CoL^3, NiL^3, and CuL^3 (Fig. S18–S20). Demetallation of the salen complex was often observed directly after preparation of the GDE: pre-electrolysis scans of CoL^2 and CoL^3 (Fig. S18) both show appreciable formation of Co(OH)$_2$, and a pre-electrolysis scan of CuL^3 (Fig. S20) shows formation of both Cu(OH)$_2$ and CuO.[13,17–20] Suspecting that interactions with the Sustainion® XA-9 binder added to the catalyst ink (in its chloride form) may lead to pre-electrolysis decomposition of our metal salen complexes, we measured UV-Vis of CoL^2 sonicated in wet ethanol both in the absence and presence of binder (Fig. S21). No significant spectral changes were observed after adding binder, suggesting that pre-electrolysis demetallation of these complexes is a result of the heating and/or desolvation incurred during dropcasting at 70 °C. We also found that demetallation of the salen complexes can occur during electrolysis under alkaline conditions. A pre-electrolysis scan of a GDE dropcast with NiL^3 shows that the salen complex remains fully intact after ink preparation and dropcasting, while the markedly different post-electrolysis scan shows Ni(OH)$_2$ as the majority species on the electrode (Fig. S19), which we attribute to the attack of hydroxide anions that have migrated through the AEM at the Ni^{II} center.[13,17] These results highlight the general need for routine spectroscopic analyses (both before and after electrolysis) to identify the species actually formed on the cathode during GDE preparation and during electrolysis.[21] In particular,
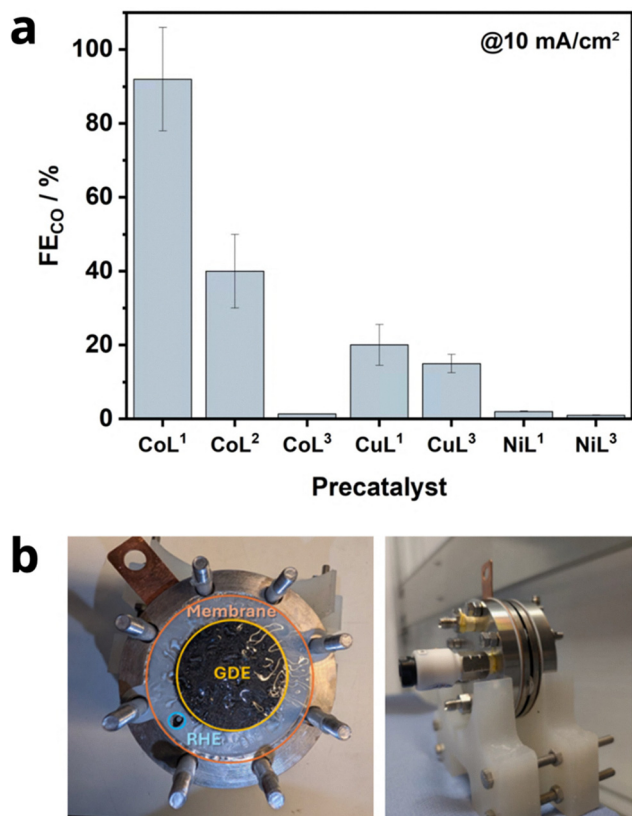
Fig. 2 (a) FE$_{CO}$ values obtained at 10 mA cm^{-2} after 30 min of electrolysis in a 2 cm^2 ZGE. Each reported FE$_{CO}$ value is the average of two separate trials, and the 95% C.I. is provided in the form of error bars. (b) Photographs of the 12 cm^2 ZGE with an integrated RHE contact used for our half-cell potential experiments.

ensuring that a targeted molecular electrocatalyst is stable at elevated pH is a key consideration when working in alkaline electrolyzers, as metal complexes (like NiL^3) that are otherwise stable to ink preparation and dropcasting steps may react with hydroxide.[15,22]

To better identify the catalytically active species actually formed on each GDE, we also performed CO_2R experiments with the simple metal salts $Co(OAc)_2$, $NiCl_2$, and $Cu(OAc)_2$ in the same metal loadings as their respective salen complexes (Fig. S29). Notably, the Ni and Cu salts outperform their respective salen complexes under identical ZGE conditions: at 10 mA cm^{-2}, we obtain FE_{CO} values of 18% for $NiCl_2$ (compare to 2% for NiL^1 and 0% for NiL^3) and 27% for $Cu(OAc)_2$ (compare to 19% for CuL^1 and 14% for CuL^3), suggesting that the metal salen complex is not the principal catalytically active species on GDEs dropcast with salen complexes of these metals. Therefore, we conclude that CuL^1 and CuL^3 primarily act as precatalysts that undergo decomposition to catalytically active $Cu(OH)_2$ or CuO species. GDEs dropcast with $Co(OAc)_2$ only evolve H_2, suggesting that the salen ligand plays a role in either (1) guiding the decomposition of CoL^1 and CoL^2 to catalytically active $Co(OH)_2$ assemblies of a particular size or shape or (2) stabilizing the Co center such that the non-decomposed complex is catalytically active.

Finally, to expand the toolbox our work offers, we fabricated a ZGE with an integrated RHE (Fig. 2b), allowing for the accurate measurement of half-cell potentials at the cathode across different current densities. The resulting half-cell potentials are plotted alongside FE_{CO} values at 10, 25, 50, and 100 mA cm^{-2} in Fig. S24–S28 for NiL^1, NiL^3, CuL^1, CuL^3, and the highest performing Co salen complex, CoL^1. We note that neither CuL^1, CuL^3, nor CoL^1 show significant voltage changes with increasing current density, suggesting the presence of conductive metallic particles performing the more kinetically favoured HER. With this approach enabling simultaneous product quantification and half-cell potential measurements in a scalable cell design, we offer the community a valuable tool for molecular electrocatalyst evaluation.

Herein, we evaluated Co, Ni, and Cu salen complexes as CO_2R precatalysts in industrially relevant ZGEs. The salen ligand is believed to play a role in the CO_2R activity of GDEs dropcast with Co salen complexes (either by directing the formation of catalytically active $Co(OH)_2$ assemblies or by stabilizing a catalytically active, non-decomposed complex), Ni salen complexes are almost entirely inactive for CO_2R, and Cu salen complexes appear to act as precatalysts that decompose to catalytically active $Cu(OH)_2$ or CuO species. FE_{CO} values were limited above 50 mA cm^{-2}, but we identify key experimental considerations for bridging lab-scale molecular electrocatalysis research and implementation in industrial electrolyzers: (1) control local water content on the GDE either at the carbon-complex interface or through CO_2 humidification, (2) apply *in situ* techniques (like surface XPS) to assess possible decomposition during ink preparation and/or electrolysis, and (3) compare GDEs dropcast with molecular complexes to those dropcast with simple metal salts to help identify active species. We also present a modified ZGE with an integrated RHE for accurately measuring half-cell potentials during electrolysis, offering molecular electrochemists another tool for probing molecular catalyst behaviour in scalable cells.

Conflicts of interest

There are no conflicts to declare.

Data availability

Notes and references

1 M. Tayyab, M. Dreis, D. Blaudszun, K. Pellumbi, U. Nzotcha, H. Tempel, M. Q. Masood, H. Weinrich, S. Stießel, K. J. Puring, R.-A. Eichel and U.-P. Apfel, *Energy Environ. Sci.*, 2025, **18**, 6854–6873.
2 W. Wiesner, K. Pellumbi, I. Zimmermann, J. Jökel, D. Siegmund and U.-P. Apfel, *Coord. Chem. Rev.*, 2025, **543**, 216909.
3 H. Bemana, M. McKee and N. Kornienko, *Chem. Sci.*, 2023, **14**, 13696–13712.
4 D. Siegmund, S. Metz, V. Peinecke, T. E. Warner, C. Cremers, A. Grevé, T. Smolinka, D. Segets and U.-P. Apfel, *JACS Au*, 2021, **1**, 527–535.
5 D. Segets, C. Andronescu and U.-P. Apfel, *Nat. Commun.*, 2023, **14**, 7950.
6 S. Singh, B. Phukan, C. Mukherjee and A. Verma, *RSC Adv.*, 2015, **5**, 3581–3589.
7 P. Bose, C. Mukherjee and A. Kumar Golder, *Chem. Eng. J.*, 2022, **431**, 134092.
8 L.-J. Zhu, D.-H. Si, F.-X. Ma, M.-J. Sun, T. Zhang and R. Cao, *ACS Catal.*, 2023, **13**, 5114–5121.
9 D. J. Pearce and D. Pletcher, *J. Electroanal. Chem.*, 1986, **194**, 317–330.
10 K. Chitchak, K. Jaisabuy and P. Vanalabhpatana, *Catal. Lett.*, 2025, **155**, 173.
11 K. Pellumbi, M.-A. Kräenbring, D. Krisch, W. Wiesner, S. Sanden, D. Siegmund, F. Özcan, K. J. Puring, R. Cao, W. Schöfberger, D. Segets and U.-P. Apfel, *Small*, 2025, **21**, e2408154.
12 L. Hoof, N. Thissen, K. Pellumbi, K. J. Puring, D. Siegmund, A. K. Mechler and U.-P. Apfel, *Cell Rep. Phys. Sci.*, 2022, **3**, 100825.
13 W. Wiesner, J. Y. Maldonado Arias, J. Jökel, R. Cao and U.-P. Apfel, *Chem. Commun.*, 2024, **60**, 14668–14671.
14 Z. Xing, L. Hu, D. S. Ripatti, X. Hu and X. Feng, *Nat. Commun.*, 2021, **12**, 136.
15 H. Chen, Z. Sun, X. Liu, A. Han and P. Du, *J. Phys. Chem. C*, 2015, **119**, 8998–9004.
16 W. Wiesner, K. Pellumbi, I. Zimmermann, J. Jökel, D. Siegmund and U.-P. Apfel, *Coord. Chem. Rev.*, 2025, **543**, 216909.
17 M. C. Biesinger, B. P. Payne, A. P. Grosvenor, L. W. M. Lau, A. R. Gerson and R. S. C. Smart, *Appl. Surf. Sci.*, 2011, **257**, 2717–2730.
18 D. Majumdar, B. Gassoumi, A. Dey, S. Roy, S. Ayachi, S. Hazra and S. Dalai, *RSC Adv.*, 2024, **14**, 14992–15007.
19 G. Ramanjaneya Reddy, S. Balasubramanian and K. Chennakesavulu, *J. Mater. Chem. A*, 2014, **2**, 15598–15610.
20 M. C. Biesinger, *Surf. Interface Anal.*, 2017, **49**, 1325–1334.
21 K. Pellumbi, D. Krisch, C. Rettenmaier, H. Awada, H. Sun, L. Song, S. A. Sanden, L. Hoof, L. Messing, K. J. Puring, D. Siegmund, B. Roldan Cuenya, W. Schöfberger and U.-P. Apfel, *Cell Rep. Phys. Sci.*, 2023, **4**, 101746.
22 T. Wu, H. Bu, S. Tao and M. Ma, *Nanoscale*, 2024, **16**, 3926–3935.